A thalamostriatal parvalbumin interneuron circuit suppresses risky reward-motivated behaviors and is disengaged by opioids

Kelsey Vollmer
Medical University of South Carolina
Lisa Green
Medical University of South Carolina
Roger Grant
Medical University of South Carolina
Kion Winston
Medical University of South Carolina
Elizabeth Doncheck
Medical University of South Carolina
Christopher Bowen
Medical University of South Carolina
Jacqueline Paniccia
Medical University of South Carolina
Rachel Clarke
Medical University of South Carolina
Annika Tiller
Medical University of South Carolina
Preston Siegler
Medical University of South Carolina
Benjamin Siemsen
Medical University of South Carolina https://orcid.org/0000-0002-6105-6054
Adam Denton
Medical University of South Carolina
Thomas Jhou
MUSC https://orcid.org/0000-0001-8811-0156
Jennifer Rinker
Medical University of South Carolina
Michael Scofield
https://orcid.org/0000-0002-2330-6999
James Otis (otis@musc.edu)

Medical University of South Carolina https://orcid.org/0000-0003-0953-9283

Article

Keywords: Reward seeking, paraventricular thalamus, nucleus accumbens, two-photon imaging, optogenetics, chemogenetics, opioids

Posted Date: April 28th, 2022

DOI: https://doi.org/10.21203/rs.3.rs-1527325/v1

Additional Declarations: There is **NO** Competing Interest.

Version of Record: A version of this preprint was published at Nature Communications on November 11th, 2022. See the published version at https://doi.org/10.1038/s41467-022-34517-w.

Title: A thalamostriatal parvalbumin interneuron circuit suppresses risky reward-motivated behaviors and is disengaged by opioids

Authors: Kelsey M. Vollmer[1]*, Lisa M. Green[1]*, Roger I. Grant[1], Kion T. Winston[1], Elizabeth M. Doncheck[1], Christopher W. Bowen[1], Jacqueline E. Paniccia[1,2], Rachel E. Clarke[1,2], Annika Tiller[1], Preston N. Siegler[1], Benjamin M. Siemsen[2], Adam R. Denton[2], Thomas C. Jhou[1], Jennifer A. Rinker[1], Michael D. Scofield[2], James M. Otis[1,3,#]

Affiliations:

[1]Department of Neuroscience, Medical University of South Carolina, Charleston, SC 29425, USA.

[2]Anesthesiology and Perioperative Medicine, Medical University of South Carolina, Charleston, SC 29425, USA.

[3]Hollings Cancer Center, Medical University of South Carolina, Charleston, SC 29425, USA.

*These authors contributed equally to this work.

[#]Corresponding author. E-mail: otis@musc.edu

Abstract:

Suppression of dangerous or inappropriate reward-motivated behaviors is critical for survival, whereas therapeutic or recreational opioid use can unleash risky behavioral actions and addiction. Nevertheless, the neuronal systems that suppress maladaptive motivated behaviors remain unclear, and whether opioids disengage those systems is unknown. Using two-photon calcium imaging *in vivo*, we identify paraventricular thalamostriatal neuronal ensembles that are inhibited upon sucrose self-administration and seeking, yet these neurons are tonically active when behavior is suppressed by a fear-provoking predator odor, a pharmacological stressor, or inhibitory learning. Electrophysiological, optogenetic, and chemogenetic experiments reveal that thalamostriatal neurons innervate accumbal parvalbumin interneurons through synapses enriched with calcium permeable AMPA receptors, and activity within this circuit is necessary and sufficient for the suppression of sucrose seeking regardless of the behavioral suppressor administered. Furthermore, systemic or intra-accumbal opioid injections rapidly dysregulate thalamostriatal ensemble dynamics, weaken thalamostriatal synaptic innervation of downstream parvalbumin interneurons, and unleash reward-seeking behaviors in a manner that is reversed by genetic deletion of thalamostriatal μ-opioid receptors. Overall, our findings reveal a thalamostriatal to parvalbumin interneuron circuit for the suppression of reward seeking that is rapidly disengaged by opioid-driven inhibition of presynaptic thalamostriatal neurons.

Keywords: Reward seeking, paraventricular thalamus, nucleus accumbens, two-photon imaging, optogenetics, chemogenetics, opioids

Introduction

Suppression of reward-seeking behaviors is critical for survival[1–3], whereas prescription or recreational opioid use can lead to unrestrained behavioral actions and opioid use disorder (OUD)[4]. Despite this knowledge, the neuronal systems that govern the suppression of reward-motivated behaviors remain unclear, and whether those systems are disengaged by opioids to unleash risky behavioral actions is unknown. The paraventricular nucleus of the thalamus (PVT) is a candidate brain region underlying opioid-gated suppression of reward seeking, as it provides an interface for motivational circuits[5–7] and has among the highest level of μ-opioid receptors of any thalamic nucleus[8]. Recent studies demonstrate that stimulation of PVT neurons can blunt feeding behaviors and promote avoidance[9–13]. Furthermore, inhibition of PVT neurons that project to the nucleus accumbens (PVT→NAc) can invigorate food seeking when food is expected but omitted[12,14]. Despite this knowledge, whether PVT→NAc circuitry provides a keystone neuronal substrate for the suppression of reward-motivated behavior, which could be provoked by a fear, stress, or inhibitory learning[15–19], is unknown. Furthermore, the neuronal mechanisms whereby opioids unleash risky behavioral actions have not been identified.

Using deep-brain two-photon calcium imaging *in vivo*, we discover PVT→NAc neuronal ensembles that display activity patterns predictive of the expression and suppression of sucrose self-administration and seeking. Electrophysiological, optogenetic, and chemogenetic studies reveal that PVT→NAc neurons pervasively govern the suppression of sucrose self-administration and seeking through the selective innervation of NAc parvalbumin interneurons at synapses enriched with calcium permeable AMPA receptors. Furthermore, we find that systemic or intra-NAc opioid exposure attenuates PVT→NAc neuronal ensemble dynamics, PVT→NAc synaptic innervation of parvalbumin interneurons, and rapidly unleashes sucrose seeking in a manner that is reversed by projection-specific inhibition of thalamostriatal μ-opioid receptors. Overall, our findings reveal a thalamostriatal feedforward inhibitory brake for reward seeking that can be rapidly disengaged by opioid-driven presynaptic inhibition.

Results

PVT→NAc Neuronal Activity is Predictive of Sucrose Taking and Seeking, and is Suppressed by Competing External Stimuli and Extinction Learning

Here we designed a paradigm that allows two-photon calcium imaging in deep brain regions during the expression and suppression of sucrose reward self-administration and seeking. Head-fixed mice were trained to press an active, but not an inactive, lever resulting in the presentation of a tone cue followed by a liquid sucrose reward (Fig. 1a-c). Suppression of active lever pressing for sucrose could be incited by the fear-provoking predator odor TMT (2,5-dihydro-2,4,5-trimethylthiazoline)[20], by the pharmacological stressor yohimbine[21], or by extinction learning wherein the cue and sucrose were omitted (Fig. 1d-f and Supplementary Fig. 1)[19]. Reward seeking could also be reinstated through cue re-exposure after extinction training (Fig. 1g). To monitor activity in PVT→NAc neurons throughout this paradigm, mice received injections of a retrogradely-trafficked virus encoding Cre-recombinase bilaterally into the NAc shell (rgAAV2-hSyn-Cre) in combination with a Cre-inducible virus encoding a calcium indicator into the posterior PVT (AAVdj-DIO-GCaMP6m[22] (Fig. 1h). Next, a microendoscopic GRIN lens was implanted dorsal to PVT, allowing chronic visual access to fluorescent GCaMP6m-expressing PVT→NAc projection neurons (Fig. 1i). Using two-photon imaging, we measured PVT→NAc neuronal activity dynamics around each active lever press after sucrose self-administration behavior was established (late in learning, days 13-14). Data revealed that PVT→NAc neuronal activity was reduced at the population level upon active lever responding for sucrose (Fig. 1j), although cell-to-cell

heterogeneity was apparent (Fig. 1k). Spectral clustering[23,24] identified three distinct PVT→NAc neuronal ensembles that could account for the response heterogeneity: those that were activated (ensemble 1), non-responding (ensemble 2), and inhibited (ensemble 3; Fig. 1l, and Supplementary Fig. 2) during each active lever press. Machine learning based behavioral decoding revealed that the PVT→NAc population dynamics could be used to predict active lever pressing during each behavioral session (Supplementary Fig. 3), and the inhibitory dynamics of neurons in ensemble 3 provided superior decoding as compared with other neurons (Fig. 1m). Next, we measured the change in basal PVT→NAc GCaMP6m fluorescence across each sucrose self-administration session, as basal fluorescence serves as a proxy for firing rates in tonically active cell populations[24,25] including PVT→NAc neurons[6]. Data revealed that within each sucrose self-administration session, the fluorescence of PVT→NAc neurons decreased across time (Fig. 1n, o). The within-session reduction was most pronounced after the behavioral task was well established (during late sessions; days 13-14), but was also present during earlier acquisition sessions (early sessions: days 1-2; middle sessions: days 7-8). Furthermore, the attenuation in activity was specific to ensembles 2 and 3 (Fig. 1p, q). Overall, both acute and tonic inhibition of select PVT→NAc neuronal ensembles predicts sucrose self-administration, consistent with the idea that activity in PVT→NAc neurons serves as a tonic 'brake' that must be released to initiate reward-motivated behavior.

We next monitored PVT→NAc neurons during the presentation of stimuli that suppress sucrose self-administration. The fear-provoking predator odor TMT and pharmacological stressor yohimbine not only prevented active lever pressing, but also prevented the inhibition of PVT→NAc neurons during sucrose self-administration (Fig. 1r, s). Additionally, while PVT→NAc neurons were inhibited when sucrose was omitted during early extinction sessions (days 1-2), this inhibition was prevented during late sessions after extinction learning was well-established (days 9-10; Fig. 1t). Thus, external stimuli and inhibitory learning that suppress sucrose self-administration and seeking also prevent the inhibition of PVT→NAc neurons. Finally, we determined if PVT→NAc neuronal inhibition could be reinstated after extinction during a cue-induced reinstatement test. Indeed, PVT→NAc neurons became tonically inhibited during cue-induced reinstatement (Fig. 1u) and showed acute, heterogeneous responses upon active lever pressing despite the absence of sucrose (Fig. 1v-w). Spectral clustering revealed qualitatively similar neuronal ensembles during cue-induced reinstatement (Fig. 1x, and Supplementary Fig. 2) as compared with previous sucrose self-administration sessions, with the inhibitory dynamics of ensemble 3 providing superior decoding of active lever pressing as compared with other ensembles (Fig. 1y-aa). Overall, sucrose self-administration and seeking are associated with ensemble-specific inhibition of PVT→NAc neurons, whereas competing behavioral suppressors prevent that inhibition. Despite these findings, whether activity in PVT→NAc is both necessary and sufficient for the suppression of reward seeking, regardless of behavioral suppressor, remains unknown.

PVT→NAc Neuronal Activity is Necessary and Sufficient for the Suppression of Sucrose Taking and Seeking

We next examined the function of PVT→NAc neuronal activity for the expression and suppression of sucrose self-administration and seeking. PVT→NAc neurons were targeted for optogenetic manipulation through injections of a retrogradely-trafficked virus encoding Cre-recombinase bilaterally into the NAc shell (rgAAV2-hSyn-Cre) in combination with viruses encoding Cre-inducible channelrhodopsin (AAV5-DIO-Ef1α-ChR2), halorhodopsin (AAV5-DIO-Ef1α-eNpHR3.0), or control enhanced yellow fluorescence protein (AAV5-DIO-Ef1α-eYFP) into the posterior PVT (Fig. 2a, b). During sucrose self-administration (Fig. 2c), optogenetic stimulation of PVT→NAc neurons in ChR2 mice decreased active lever pressing (Fig. 2d, e) akin to previous findings[11,14]. Furthermore, while the

predator odor TMT or pharmacological stressor yohimbine suppressed sucrose self-administration in control eYFP mice, inhibition of PVT→NAc neurons prevented that behavioral suppression in eNpHR mice (Fig. 2f, g). Similarly, while extinction training suppressed active lever pressing in the absence of sucrose, the inhibition of PVT→NAc neurons unleashed active lever pressing (Fig. 2h). Finally, after extinction learning we found that cue-induced reinstatement of sucrose seeking was suppressed by the stimulation of PVT→NAc neurons (Fig. 2i). Importantly, the behavioral effects of PVT→NAc stimulation and inhibition were specific to the active but not inactive lever (Supplementary Fig. 1), suggesting that the optogenetic manipulations adjusted goal-directed behavioral output. In further support of this specificity, we found that PVT→NAc stimulation did not inhibit locomotor activity, despite provoking a real-time place aversion (Supplementary Fig. 4) as previously reported[13]. Together, these data reveal that PVT→NAc neuronal activity is both necessary and sufficient for the suppression of sucrose self-administration and seeking, an effect that is generalizable across behavioral suppressors.

PVT→NAc-dependent Suppression of Reward Seeking Requires Downstream CP-AMPARs and PV Interneurons

We next identified candidate downstream cellular targets that may underlie thalamostriatal-dependent suppression of reward seeking. Following injections of an anterogradely trafficked transsynaptic AAV1 virus expressing Cre (AAV1-CamKII-Cre)[26–28] in the posterior PVT, we infused a Cre-dependent virus encoding eYFP bilaterally in the NAc (AAV5-ef1α-DIO-eYFP). Following incubation, we performed immunohistochemistry for eYFP in combination with immunohistochemistry for known NAc cell types in *ex vivo* brain slices (Supplementary Fig. 5). Overall, experiments confirmed that putative dopamine 1 receptor and dopamine 2 receptor expressing medium spiny neurons in the NAc shell are synaptically innervated by PVT (PVT→NAc$^{D1\text{-}MSNs}$; PVT→NAc$^{D2\text{-}MSNs}$). We also found elevated anterograde transsynaptic labeling of parvalbumin-expressing interneurons in the NAc shell (PVT→NAc$^{PV\text{-}INs}$) as compared with other striatal interneurons, a finding consistent with a previous electrophysiological study showing functional input from PVT to striatal PV interneurons[29]. To further characterize PVT synaptic innervation of D1-MSNs, D2-MSNs, and PV-INs, we injected a virus encoding the red-shifted excitatory opsin ChrimsonR (AAV5-hSyn-ChrR)[30] into PVT and a Cre-inducible virus encoding eYFP (AAV5-ef1α-DIO-eYFP) into the NAc shell of Cre-driver mouse lines (D2-Cre; PV-Cre; Fig. 3a, b). Subsequent patch-clamp electrophysiological recordings revealed elevated glutamatergic excitatory synaptic drive at PVT→NAc$^{PV\text{-}IN}$ synapses as compared with PVT→NAc$^{D1\text{-}MSN}$ and PVT→NAc$^{D2\text{-}MSN}$ synapses (Fig. 3c, d). Additionally, we found that PVT→NAc$^{PV\text{-}IN}$ synapses were inwardly rectifying, whereas other synapses were not (Fig. 3e, f). Inwardly rectifying glutamatergic synapses suggest the presence of calcium-permeable AMPA receptors (CP-AMPARs), which are known to be selectively enriched in striatal PV interneurons[31]. Indeed, we found that pharmacological inhibition of CP-AMPARs selectively attenuated excitatory synaptic drive at PVT→NAc$^{PV\text{-}IN}$ synapses, but not PVT→NAc$^{D2\text{-}MSN}$ or putative PVT→NAc$^{D1\text{-}MSN}$ synapses (Fig. 3g, h). Altogether, PVT→NAc projection neurons have biased innervation of PV interneurons at synapses enriched with CP-AMPARs, however the function of this synaptic connectivity for the suppression of reward seeking remains unknown.

We next determined the necessity of cell-type biased signaling mechanisms for PVT→NAc dependent suppression of reward seeking. To do so, we replicated the above behavioral optogenetics experiment (shown in Fig. 2) but implanted a bilateral cannula dorsal to the NAc shell allowing simultaneous neuropharmacological manipulation (Fig. 3i). Optogenetic stimulation of PVT→NAc neurons suppressed sucrose self-administration as above, and pharmacological inhibition of D1 or D2 receptor signaling did not rescue lever pressing behavior. In contrast, inhibition of NAc CP-AMPARs selectively rescued active lever pressing, despite optogenetic stimulation of PVT→NAc neurons (Fig. 3j, and Supplementary Fig. 1). Considering that PVT→NAc$^{PV\text{-}IN}$ synapses have enriched CP-AMPARs,

we next used chemogenetics to determine the necessity of PV interneuron activation for the suppression of sucrose self-administration (Fig. 3k). Following a similar surgical design as above, we injected a Cre-inducible virus encoding an inhibitory DREADD (AAV5-hSyn-DIO-hM4D(Gi)-mCherry) bilaterally in the NAc of transgenic PV-Cre mice. Chemogenetic inhibition of NAc PV interneurons prevented the suppression of sucrose self-administration caused by optogenetic stimulation of PVT→NAc neurons (Fig. 3l), by presentation of the predator odor TMT (Fig. 3m), by the pharmacological stressor yohimbine (Fig. 3n), and by extinction learning (Fig. 3o). In contrast, these manipulations did not affect inactive lever pressing (Supplementary Fig. 1). Thus, PVT→NAc dependent suppression of reward seeking requires activity at downstream CP-AMPARs and PV interneurons. Whether this keystone feedforward inhibitory circuit for the suppression of reward seeking is modulated by opioids, however, remains unclear.

PVT→NAc-dependent Suppression of Reward Seeking is Gated by Presynaptic μ-Opioid Receptors.

Opioid use disorder is associated with maladaptive reward-seeking behaviors despite negative consequences[32–35]. Despite this knowledge, whether a single opioid experience can unleash reward-seeking behaviors in the face of competing behavioral suppressors remains unknown. Through combinatorial viral labeling and immunohistochemistry, we observed the co-expression of μ-opioid recpetors with PVT→NAc somata and terminal axons (Fig. 4a, b), suggesting that the PVT→NAc brake for reward seeking may be tightly regulated by opioidergic activity. To investigate this possibility, mice were given a single injection of the opioid heroin during two-photon calcium imaging of PVT→NAc neurons. Systemic heroin reliably reduced the activity of these neurons (Fig. 4c, d). Furthermore, when heroin was administered prior to a sucrose self-administration session, PVT→NAc neuronal ensembles were altered such that a smaller proportion of neurons displayed excitatory (ensemble 1) or inhibitory (ensemble 3) dynamics, reducing the ability of these neurons to decode active lever pressing behavior (Fig. 4e-h, and Supplementary Fig. 6). Finally, we determined the influence of heroin on PVT→NAc-dependent behavioral suppression. Heroin not only prevented the suppression of sucrose self-administration caused by optogenetic stimulation of PVT→NAc neurons (Fig. 4i), but also by the predator odor TMT (Fig. 4j) and pharmacological stressor yohimbine (Fig. 4k). Surprisingly, heroin also caused PVT→NAc stimulation to be appetitive, rather than aversive, as mice expressed a stimulation-dependent real-time place preference (Supplementary Fig. 4). Thus, a single dose of the opioid heroin attenuated PVT→NAc ensemble dynamics and prevented the suppression of reward seeking.

We next determined whether local μ-OR activity was responsible for heroin-dependent behavioral disinhibition. To do so, we replicated previous behavioral optogenetics experiments (shown in Figs. 2 and 3) but implanted a bilateral cannula dorsal to the NAc shell, allowing for simultaneous pharmacological manipulation of μ-opioid receptors using the selective agonist DAMGO ([D-Ala^2, NMePhe^4, Gly-ol]-enkephalin; Fig. 5a). Optogenetic stimulation of PVT→NAc neurons suppressed sucrose self-administration as above, however, this effect was blocked by intra-NAc infusion of DAMGO (Fig. 5b). Furthermore, DAMGO prevented the behavioral suppression caused by predator odor TMT exposure (Fig. 5c), and by the pharmacological stressor yohimbine (Fig. 5d). Additionally, heroin and DAMGO-mediated rescue of lever pressing was goal-directed, as inactive lever pressing was unchanged (Supplementary Fig. 1). We next investigated whether PVT synaptic innervation of NAc PV interneurons was sensitive to local μ-OR activity. Similar to the viral strategy above (see Fig. 3), we injected a virus encoding the excitatory opsin ChrimsonR (AAV5-hSyn-ChrR)[30] into PVT and a Cre-inducible virus encoding eYFP (AAV5-ef1α-DIO-eYFP) into the NAc shell of PV-Cre transgenic mice (Fig. 5e). Using *ex vivo* patch clamp electrophysiology, we found that bath application of DAMGO

decreased glutamatergic excitatory synaptic drive at PVT→NAc$^{PV\text{-}IN}$ synapses (Fig. 5f), suggesting that μ-OR activity may prevent PVT→NAc-dependent suppression of reward seeking through a presynaptic mechanism. Thus, we determined whether PVT→NAc μ-OR activity was necessary for preventing behavioral suppression. To do so, we used transgenic *Oprm1*$^{fl/fl}$ mice, which have *loxP* sites flanking exons 2-3 of the *Oprm1* gene for cre-dependent knockout of μ -ORs. *Oprm1*$^{fl/fl}$ and wildtype (WT) mice received injections of a virus encoding Cre-recombinase (AAV5-hSyn-Cre) into PVT, and bilateral injections of a retrogradely-trafficked virus encoding channelrhodopsin (rgAAV2-hSyn-ChR2-eYFP) into NAc shell. Additionally, an optical fiber was implanted dorsal to PVT, and a bilateral cannula was implanted dorsal to NAc shell (Fig. 5g). Similar to above, we found that an intra-NAc infusion of DAMGO prevented the suppression of sucrose self-administration caused by optogenetic stimulation in WT mice. However, knockout of PVT μ-ORs in *Oprm1*$^{fl/fl}$ mice rescued optogenetically-evoked behavioral suppression in the presence of NAc DAMGO (Fig. 5f). Inactive lever pressing did not change across groups or conditions (Supplementary Fig. 1). Overall, these data reveal that PVT→NAc neurons and PVT→NAc dependent behaviors are tightly regulated by local, presynaptic PVT→NAc μ-ORs.

Discussion

Here we identify PVT→NAc neuronal ensembles that have acute and tonic activity patterns predictive of the expression and suppression of sucrose self-administration and seeking. These activity dynamics are necessary and sufficient for the suppression of sucrose seeking, causally mediated through downstream PV interneurons and CP-AMPARs which are selectively enriched at PVT→NAc$^{PV\text{-}IN}$ synapses. We find that systemic or local NAc opioid injections reduce both PVT→NAc neuronal ensemble dynamics and synaptic innervation of PV interneurons, unleashing sucrose seeking in the face of competing behavioral suppressors through presynaptic inhibition. Overall, we discover a keystone neuronal system for the suppression of reward-motivated behaviors and find that this system is rapidly disengaged by opioids.

Akin to our findings, previous studies show that stimulation of PVT can prevent feeding and promote avoidance[9–13], whereas inhibition of PVT neurons can promote reward seeking when food is expected but omitted[12,14]. Surprisingly, here we find that PVT→NAc neurons play a pervasive role in the suppression of reward-motivated behavior, and through an unexpected synaptic input to NAc PV interneurons. Other studies have focused on the role of PVT synaptic input to NAc D1- and D2-MSNs[13,36,37], and have found unique functions of these pathways in other behaviors such as the expression of opioid withdrawal[13] and the retrieval of an opioid conditioned place preference memory[37]. Thus, discrete outputs from PVT to unique NAc cell types likely control distinct behavioral states, including the suppression of reward seeking as described here.

Here we find that the PVT→NAc to PV interneuron brake for reward seeking is highly sensitive to opioids. Consistently, previous studies reveal that accumbal μ-opioid receptors can promote feeding [38–40], and can facilitate drug-seeking behaviors[41–43]. Our findings suggest that these behavioral effects could be, at least in part, related to the inhibition of PVT→NAc to PV interneuron circuitry – disinhibiting the reward-motivated behavioral actions. In contrast, studies evaluating the function of PVT→NAc neuronal activity for opioid seeking in the self-administration paradigm have remained mixed. A recent study showed that stimulation of this pathway can modestly increase opioid seeking before, but not after, extinction learning[36]. In contrast, others showed that activation of this pathway can increase opioid seeking, but only under conditions of chronic food restriction[44]. Considering the ability of opioids to disengage PVT→NAc to PV interneuron circuitry, it is possible that chronic opioid experience causes long-lasting adaptations at PVT→NAc synapses that could disrupt the ability of this circuit to suppress operant behaviors including opioid seeking. Future studies that evaluate cell-type specific adaptations

within the PVT→NAc to PV interneuron circuit following heroin self-administration are therefore warranted.

Our two-photon calcium imaging data highlights the heterogeneous, although overall inhibitory, PVT→NAc neuronal ensemble dynamics during sucrose self-administration and seeking. While we isolate PVT neurons by location (i.e., posterior) and connection (i.e., projections to NAc), neuronal ensembles with unique activity patterns still arise. Previous research has shown that unique PVT cell types can have opposing effects on behavior, as this structure contains many classes of neurons that can be distinguished by anatomical location (anterior versus posterior)[45–48], function[9,49,50], and gene expression[46,51]. While we find that PVT→NAc neuronal activity is modulated by μ-opioid receptor activity, there are an abundance of genotypic differences that have yet to be explored; moreover, whether these genotypic differences contribute to the heterogenous activity in PVT→NAc neuronal ensembles remains unclear. Future studies including high-throughput single-cell sequencing or targeting of unique cell types would aid in elucidating how these genetically distinct cell populations contribute to reward-seeking behavior.

Overall, we discover a keystone neuronal system for behavioral suppression and show that this system is rapidly disengaged by opioids. These findings provide a neuronal substrate whereby prescription or recreational opioid could lead to risky motivated behavioral actions and addiction. Newly synthesized opioids or competing pharmacologies that prevent the inhibition of thalamostriatal circuits could therefore reduce a patient's vulnerability to addiction.

Acknowledgements

We would like to thank Dr. Jacqueline McGinty and Maribel Vasquez-Silva for technical advice and support. This study was funded by grants from the National Institute of Drug Abuse (NIDA), F31-DA052186 (KMV), F32-DA053830 (EMD), R01-DA051650 (JMO), R01-DA054154 (MDS), T32-DA007288 (RIG, JEP), F32-DA050427 (BMS), R25-GM113278 (PNS, KTW), and the MUSC College of Medicine (COMETS; JMO and MDS).

Author Contributions

KMV, LMG, MDS, and JMO designed the experiments and wrote the manuscript. All authors provided technical assistance and provided intellectual feedback on the project.

Competing Interests

The authors have no competing interests to declare.

References

1. Logan, G. D. Executive control of thought and action. *Acta Psychol. (Amst.)* **60**, 193–210 (1985).
2. Mansouri, F. A., Tanaka, K. & Buckley, M. J. Conflict-induced behavioural adjustment: a clue to the executive functions of the prefrontal cortex. *Nat. Rev. Neurosci.* **10**, 141–152 (2009).
3. Stephens, D. W. & Krebs, J. R. *Foraging theory*. (Princeton University Press, 1986).
4. Webster, L. R. Risk Factors for Opioid-Use Disorder and Overdose. *Anesth. Analg.* **125**, 1741–1748 (2017).
5. Kirouac, G. J. Placing the paraventricular nucleus of the thalamus within the brain circuits that control behavior. *Neurosci. Biobehav. Rev.* **56**, 315–329 (2015).
6. Otis, J. M. *et al.* Paraventricular Thalamus Projection Neurons Integrate Cortical and Hypothalamic Signals for Cue-Reward Processing. *Neuron* **103**, 423-431.e4 (2019).
7. Kelley, A. E., Baldo, B. A. & Pratt, W. E. A proposed hypothalamic–thalamic–striatal axis for the integration of energy balance, arousal, and food reward. *J. Comp. Neurol.* **493**, 72–85 (2005).
8. Ding, Y.-Q., Kaneko, T., Nomura, S. & Mizuno, N. Immunohistochemical localization of μ-opioid receptors in the central nervous system of the rat. *J. Comp. Neurol.* **367**, 375–402 (1996).
9. Choi, E. A. & McNally, G. P. Paraventricular Thalamus Balances Danger and Reward. *J. Neurosci.* **37**, 3018–3029 (2017).
10. Choi, E. A., Jean-Richard-dit-Bressel, P., Clifford, C. W. G. & McNally, G. P. Paraventricular Thalamus Controls Behavior during Motivational Conflict. *J. Neurosci.* **39**, 4945–4958 (2019).
11. Engelke, D. S. *et al.* A hypothalamic-thalamostriatal circuit that controls approach-avoidance conflict in rats. *Nat. Commun.* **12**, 2517 (2021).
12. Lafferty, C. K., Yang, A. K., Mendoza, J. A. & Britt, J. P. Nucleus Accumbens Cell Type- and Input-Specific Suppression of Unproductive Reward Seeking. *Cell Rep.* **30**, 3729-3742.e3 (2020).
13. Zhu, Y., Wienecke, C. F. R., Nachtrab, G. & Chen, X. A thalamic input to the nucleus accumbens mediates opiate dependence. *Nature* **530**, 219–222 (2016).
14. Do-Monte, F. H., Minier-Toribio, A., Quiñones-Laracuente, K., Medina-Colón, E. M. & Quirk, G. J. Thalamic Regulation of Sucrose Seeking during Unexpected Reward Omission. *Neuron* **94**, 388-400.e4 (2017).
15. Walasek, G., Wqsierska, M. & Zielinski, K. Conditioning of fear and conditioning of safety in rats. 12.
16. Apfelbach, R., Blanchard, C. D., Blanchard, R. J., Hayes, R. A. & McGregor, I. S. The effects of predator odors in mammalian prey species: a review of field and laboratory studies. *Neurosci. Biobehav. Rev.* **29**, 1123–1144 (2005).

17. Armario, A. The Hypothalamic-Pituitary-Adrenal Axis: What can it Tell us About Stressors? *CNS Neurol. Disord. - Drug Targets* **5**, 485–501.
18. Harkness, J. H., Wells, J., Webb, S. & Grimm, J. W. Extended exposure to environmental cues, but not to sucrose, reduces sucrose cue reactivity in rats. *Learn. Behav.* **44**, 59–66 (2016).
19. Peters, J., Kalivas, P. W. & Quirk, G. J. Extinction circuits for fear and addiction overlap in prefrontal cortex. *Learn. Mem.* **16**, 279–288 (2009).
20. Janitzky, K., D'Hanis, W., Kröber, A. & Schwegler, H. TMT predator odor activated neural circuit in C57BL/6J mice indicates TMT-stress as a suitable model for uncontrollable intense stress. *Brain Res.* **1599**, 1–8 (2015).
21. Davis, M., Redmond, D. E. & Baraban, J. M. Noradrenergic agonists and antagonists: Effects on conditioned fear as measured by the potentiated startle paradigm. *Psychopharmacology (Berl.)* **65**, 111–118 (1979).
22. Chen, T.-W. *et al.* Ultrasensitive fluorescent proteins for imaging neuronal activity. *Nature* **499**, 295–300 (2013).
23. Grant, R. I. *et al.* Specialized coding patterns among dorsomedial prefrontal neuronal ensembles predict conditioned reward seeking. *eLife* **10**, e65764 (2021).
24. Namboodiri, V. M. K. *et al.* Single-cell activity tracking reveals that orbitofrontal neurons acquire and maintain a long-term memory to guide behavioral adaptation. *Nat. Neurosci.* **22**, 1110–1121 (2019).
25. Otis, J. M. *et al.* Prefrontal cortex output circuits guide reward seeking through divergent cue encoding. *Nature* **543**, 103–107 (2017).
26. Weinholtz, C. A. & Castle, M. J. Intersectional targeting of defined neural circuits by adeno-associated virus vectors. *J. Neurosci. Res.* **99**, 981–990 (2021).
27. Zingg, B., Peng, B., Huang, J., Tao, H. W. & Zhang, L. I. Synaptic Specificity and Application of Anterograde Transsynaptic AAV for Probing Neural Circuitry. *J. Neurosci.* **40**, 3250–3267 (2020).
28. Zingg, B. *et al.* AAV-Mediated Anterograde Transsynaptic Tagging: Mapping Corticocollicular Input-Defined Neural Pathways for Defense Behaviors. *Neuron* **93**, 33–47 (2017).
29. Yu, J. *et al.* Nucleus accumbens feedforward inhibition circuit promotes cocaine self-administration. *Proc. Natl. Acad. Sci.* **114**, E8750–E8759 (2017).
30. Klapoetke, N. C. *et al.* Independent optical excitation of distinct neural populations. *Nat. Methods* **11**, 338–346 (2014).
31. Gittis, A. H. *et al.* Selective Inhibition of Striatal Fast-Spiking Interneurons Causes Dyskinesias. *J. Neurosci.* **31**, 15727–15731 (2011).
32. Kalivas, P. W. & Volkow, N. D. The Neural Basis of Addiction: A Pathology of Motivation and Choice. *Am. J. Psychiatry* **162**, 1403–1413 (2005).

33. Koob, G. F. & Le Moal, M. Drug abuse: hedonic homeostatic dysregulation. *Science* **278**, 52–58 (1997).
34. Koob, G. F. & Le Moal, M. Addiction and the Brain Antireward System. *Annu. Rev. Psychol.* **59**, 29–53 (2008).
35. Koob, G. F. & Volkow, N. D. Neurobiology of addiction: a neurocircuitry analysis. *Lancet Psychiatry* **3**, 760–773 (2016).
36. Giannotti, G. *et al.* Extinction blunts paraventricular thalamic contributions to heroin relapse. *Cell Rep.* **36**, 109605 (2021).
37. Keyes, P. C. *et al.* Orchestrating Opiate-Associated Memories in Thalamic Circuits. *Neuron* **107**, 1113-1123.e4 (2020).
38. Castro, D. C. *et al.* An endogenous opioid circuit determines state-dependent reward consumption. *Nature* **598**, 646–651 (2021).
39. Majeed, N. H., Przewklocka, B., Wędzony, K. & Przewklocki, R. Stimulation of food intake following opioid microinjection into the nucleus accumbens septi in rats. *Peptides* **7**, 711–716 (1986).
40. Zhang, M. & Kelley, A. E. Enhanced intake of high-fat food following striatal mu-opioid stimulation: microinjection mapping and Fos expression. *Neuroscience* **99**, 267–277 (2000).
41. Koob, G. F., Vaccarino, F. J., Amalric, M. & Bloom, F. E. Neurochemical substrates for opiate reinforcement. *NIDA Res. Monogr.* **71**, 146–164 (1986).
42. Richard, J. M. & Fields, H. L. Mu-opioid receptor activation in the medial shell of nucleus accumbens promotes alcohol consumption, self-administration and cue-induced reinstatement. *Neuropharmacology* **108**, 14–23 (2016).
43. Simmons, D. & Self, D. W. Role of Mu and Delta Opioid Receptors in the Nucleus Accumbens in Cocaine-Seeking Behavior. *Neuropsychopharmacol. Off. Publ. Am. Coll. Neuropsychopharmacol.* **34**, 1946–1957 (2009).
44. Chisholm, A. *et al.* Assessing the Role of Corticothalamic and Thalamo-Accumbens Projections in the Augmentation of Heroin Seeking in Chronically Food-Restricted Rats. *J. Neurosci.* **41**, 354–365 (2021).
45. Dong, X., Li, S. & Kirouac, G. J. Collateralization of projections from the paraventricular nucleus of the thalamus to the nucleus accumbens, bed nucleus of the stria terminalis, and central nucleus of the amygdala. *Brain Struct. Funct.* **222**, 3927–3943 (2017).
46. Gao, C. *et al.* Two genetically, anatomically and functionally distinct cell types segregate across anteroposterior axis of paraventricular thalamus. *Nat. Neurosci.* **23**, 217–228 (2020).
47. Li, S. & Kirouac, G. J. Projections from the paraventricular nucleus of the thalamus to the forebrain, with special emphasis on the extended amygdala. *J. Comp. Neurol.* **506**, 263–287 (2008).

48. Penzo, M. A. *et al.* The paraventricular thalamus controls a central amygdala fear circuit. *Nature* **519**, 455–459 (2015).
49. Beas, B. S. *et al.* The locus coeruleus drives disinhibition in the midline thalamus via a dopaminergic mechanism. *Nat. Neurosci.* **21**, 963–973 (2018).
50. Flagel, S. B. *et al.* A FOOD PREDICTIVE CUE MUST BE ATTRIBUTED WITH INCENTIVE SALIENCE FOR IT TO INDUCE c-FOS mRNA EXPRESSION IN CORTICO-STRIATAL-THALAMIC BRAIN REGIONS. *Neuroscience* **196**, 80–96 (2011).
51. McGinty, J. F. & Otis, J. M. Heterogeneity in the Paraventricular Thalamus: The Traffic Light of Motivated Behaviors. *Front. Behav. Neurosci.* **14**, 181 (2020).
52. Madisen, L. *et al.* A robust and high-throughput Cre reporting and characterization system for the whole mouse brain. *Nat. Neurosci.* **13**, 133–140 (2010).
53. Gong, S. *et al.* Targeting Cre recombinase to specific neuron populations with bacterial artificial chromosome constructs. *J. Neurosci. Off. J. Soc. Neurosci.* **27**, 9817–9823 (2007).
54. Weibel, R. *et al.* Mu Opioid Receptors on Primary Afferent Nav1.8 Neurons Contribute to Opiate-Induced Analgesia: Insight from Conditional Knockout Mice. *PLoS ONE* **8**, e74706 (2013).
55. Resendez, S. L. *et al.* Visualization of cortical, subcortical and deep brain neural circuit dynamics during naturalistic mammalian behavior with head-mounted microscopes and chronically implanted lenses. *Nat. Protoc.* **11**, 566–597 (2016).
56. Mahler, S. V. *et al.* Chemogenetic Manipulations of Ventral Tegmental Area Dopamine Neurons Reveal Multifaceted Roles in Cocaine Abuse. *J. Neurosci.* **39**, 503–518 (2019).
57. Zhu, H. *et al.* Cre dependent DREADD (Designer Receptors Exclusively Activated by Designer Drugs) mice. *Genes. N. Y. N 2000* **54**, 439–446 (2016).
58. Sparta, D. R. *et al.* Construction of implantable optical fibers for long-term optogenetic manipulation of neural circuits. *Nat. Protoc.* **7**, 12–23 (2012).
59. Vollmer, K. M. *et al.* A Novel Assay Allowing Drug Self-Administration, Extinction, and Reinstatement Testing in Head-Restrained Mice. *Front. Behav. Neurosci.* **15**, 258 (2021).
60. King, C. E. & Becker, H. C. Oxytocin attenuates stress-induced reinstatement of alcohol seeking behavior in male and female mice. *Psychopharmacology (Berl.)* **236**, 2613–2622 (2019).
61. Kaifosh, P., Zaremba, J. D., Danielson, N. B. & Losonczy, A. SIMA: Python software for analysis of dynamic fluorescence imaging data. *Front. Neuroinformatics* **8**, (2014).
62. Schindelin, J. *et al.* Fiji: an open-source platform for biological-image analysis. *Nat. Methods* **9**, 676–682 (2012).
63. Stuber, G. D. *et al.* Excitatory transmission from the amygdala to nucleus accumbens facilitates reward seeking. *Nature* **475**, 377–380 (2011).
64. Chen, Z. *et al.* Dynorphin activation of kappa opioid receptor reduces neuronal excitability in the paraventricular nucleus of mouse thalamus. *Neuropharmacology* **97**, 259–269 (2015).

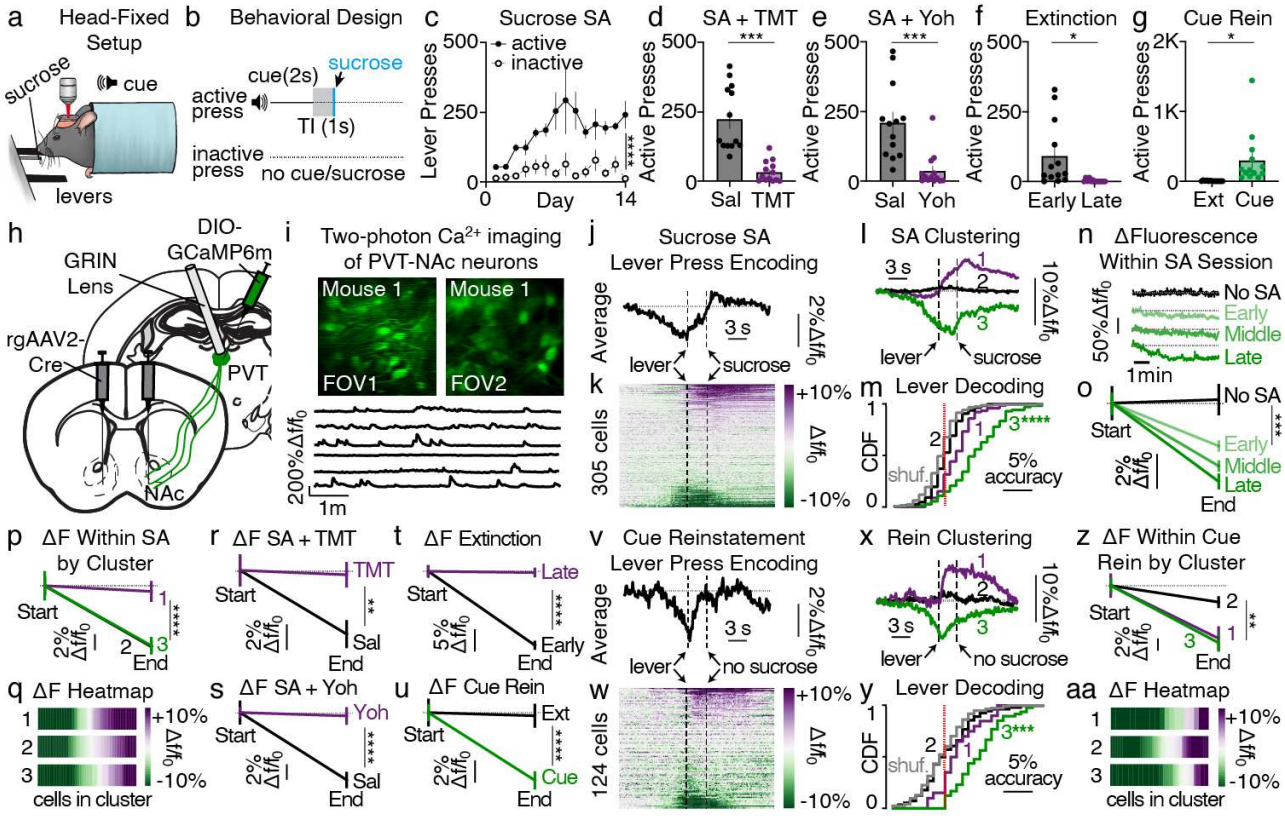

Figure 1. Inhibition of select PVT→NAc neuronal ensembles predicts sucrose self-administration and seeking.

a-c, Head-fixed design (**a**), behavioral schematic (**b**), and grouped data (**c**) for acquisition of sucrose self-administration (n=13 mice; lever: $F_{1,24}$=60.65, P<0.001). **d-f,** TMT (**d**), yohimbine (**e**), and extinction (**f**) suppressed active lever pressing (TMT: t_{12}=5.54; yohimbine: t_{12}=5.66; extinction: t_{12}=2.72). **g**, Cue exposure provoked reinstatement of active lever pressing after extinction (t_{12}=2.79). **h**,**i**, Surgical strategy (**h**) for visualization of PVT→NAc projection neurons (**i**; top) and calcium-mediated fluorescent signal extraction (**i**; bottom). **j**,**k**, Averaged trace (**j**) and single-cell heatmap (**k**) revealing PVT→NAc dynamics during sucrose self-administration (n=6 mice, 305 neurons). **l**, Clustering reveals three PVT→NAc neuronal ensembles that emerge during sucrose self-administration: excitatory responders, non-responders, and inhibitory responders. **m**, Active lever press decoding was most accurate for ensemble 3 during self-administration (interaction: $F_{2,604}$=34.02, P<0.0001). **n**,**o**, Example waveforms (**n**) and grouped data (**o**) showing reduced PVT→NAc activity during each self-administration session but not a baseline (No-SA) session (interaction: $F_{3,2116}$=5.19, P=0.001; n=3-6 mice; 105-327 neurons per session). **p**,**q**, Grouped data (**p**) and heatmap (**q**) reveal within-session reductions in activity for each ensemble (interaction: $F_{2,604}$=4.99, P=0.007). **r-t**, TMT (**r**), yohimbine (**s**), and extinction (**t**) prevented within-session reductions in PVT→NAc activity (interactions: F-values>4.0; 66-150 neurons per session). **u,** PVT→NAc activity was reduced during cue-induced reinstatement (interaction: $F_{1,544}$=7.83, P=0.005; n=124 neurons). **v**,**w**, Averaged trace (**v**) and corresponding heatmap (**w**) revealing PVT→NAc dynamics during cue-induced reinstatement. **x**, Clustering reveals three PVT→NAc neuronal ensembles during reinstatement. **y**, Active lever press decoding was most accurate for ensemble 3 during reinstatement (interaction: $F_{2,242}$=8.23, P=0.0004). **z**,**aa**, Grouped data (**z**) and heatmap (**aa**) reveal within-session reduction in activity for each ensemble during cue-induced reinstatement (interaction: $F_{2,242}$=4.27, P=0.015). TI, trace interval; FOV, field of view; SA, self-administration; Rein, reinstatement; Yoh, yohimbine. Group comparisons: *P<0.05, **P<0.01, ***P=0.001, ****P<0.001.

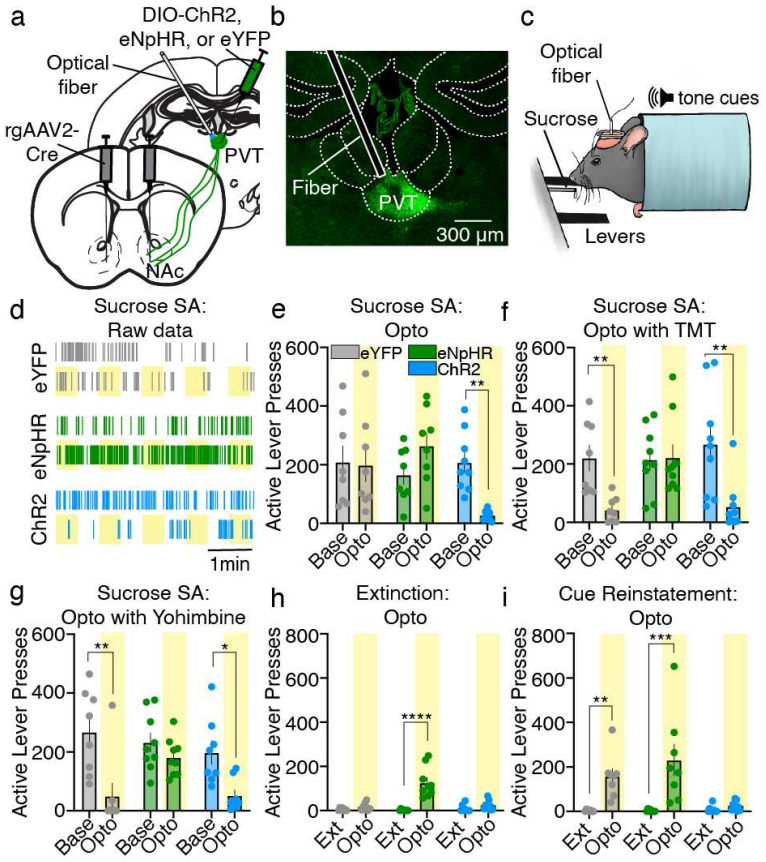

Figure 2. PVT→NAc activity dynamics are necessary and sufficient for the expression and suppression of sucrose self-administration and seeking.

a-c, Surgical strategy (**a**) for optogenetic manipulation of PVT→NAc neurons (**b**) during sucrose self-administration (**c**). **d**, Raster plot showing example active lever pressing rates in each group during sucrose self-administration (examples from 5 mice/group; yellow bar=light on). **e**, Group data showing that optogenetic stimulation of PVT→NAc neurons suppressed active lever pressing (n=8-9 mice/group; interaction: $F_{2,22}$=7.09, *P*=0.004). **f-h**, TMT (**f**), yohimbine (**g**), and extinction (**h**) suppressed active lever pressing, whereas inhibition of PVT→NAc neurons in eNpHR mice rescued active lever pressing (TMT: interaction: $F_{2,23}$=5.36, P=0.01; yohimbine: day: $F_{1,22}$=20.46, *P*=0.002; extinction: interaction: $F_{2,23}$=19.55, P<0.001). **i**, Cue-induced reinstatement of active lever pressing after extinction was abolished by stimulation of PVT→NAc neurons in ChR2 mice (interaction: $F_{2,22}$=6.15, *P*=0.008). Ext, extinction; Opto, optogenetic manipulation; SA, self-administration. Group comparisons: **P*<0.05, ***P*<0.01, ****P*=0.001, *****P*<0.001.

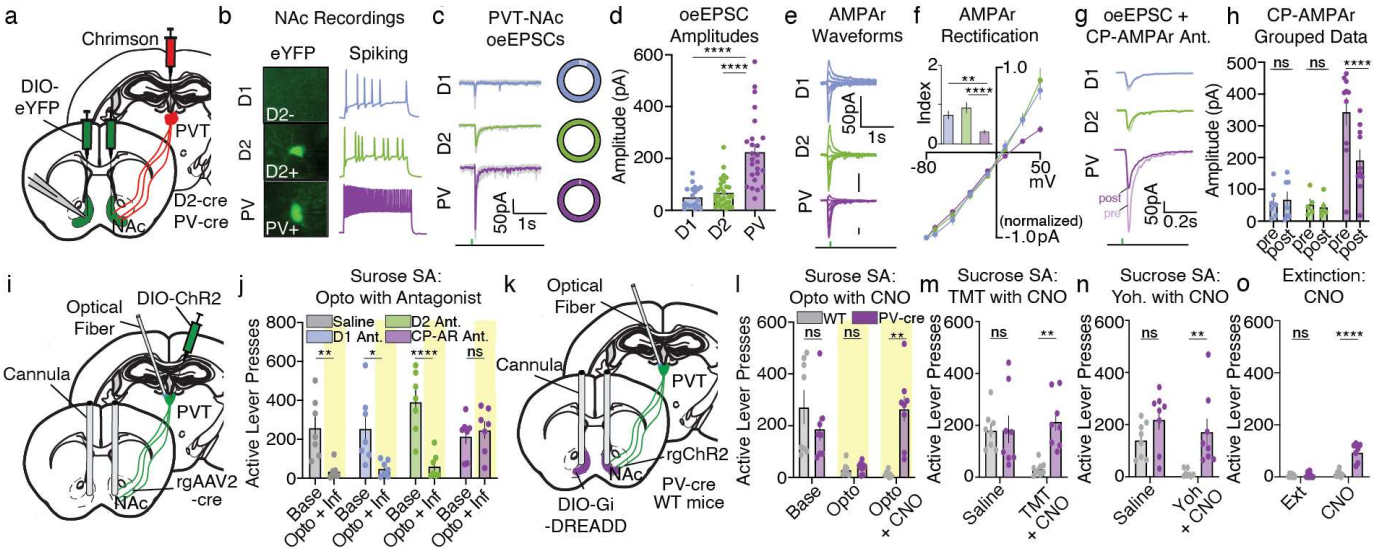

Figure 3. PVT→NAc dependent suppression of reward seeking requires downstream CP-AMPARs and PV interneurons.

a, Surgical strategy for patch-clamp electrophysiology. **b**, Example fluorescent images (left) and action potential traces (right) for identification of NAc cell types. **c**,**d**, Example waveforms (**c**; pie charts show % responding neurons) and grouped data (**d**) reveal elevated oeEPSC amplitudes in NAc PV-INs (n=20-28 cells; 8-11 mice/group; $F_{2,69=}27.78$, $P<0.001$). **e**,**f**, Example waveforms (**e**) and grouped data (**f**) showing that PVT→NAc$^{PV\text{-}IN}$ synapses are selectively inwardly rectifying (n=10-16 cells; 5-7 mice/group). Inset: rectification index ($I_{50}/-I_{-70}$; $F_{2,34=}13.27$, $P<0.001$). **g**,**h**, Waveforms (**g**) and grouped data (**h**) showing that bath application of the CP-AMPAr antagonist IEM-1640 selectively reduced oeEPSC amplitudes at PVT→NAc$^{PV\text{-}IN}$ synapses (n=5-10 cells, 4-5 mice/group; interaction: $F_{2,19=}13.17$, P=0.003). **i**, Surgical strategy for simultaneous optogenetic manipulation of PVT→NAc neurons and intra-NAc neuropharmacology. **j**, Microinfusions of the CP-AMPAr antagonist prevented the suppression of sucrose self-administration caused by stimulation of PVT→NAc neurons (n=7 mice/group; interaction: $F_{3,24}=5.98$, $P=0.003$). **k**, Surgical strategy for simultaneous optogenetic stimulation of PVT→NAc neurons and chemogenetic inhibition of PV-INs. **l**, Chemogenetic inhibition of PV-INs through intra-NAc infusions of CNO in PV-Cre mice, but not WT mice, prevented the suppression of sucrose self-administration caused by optogenetic stimulation of PVT→NAc neurons (n=7-8 mice/group; interaction: $F_{2,28=}11.33$, $P<0.001$). **m**-**o**, Chemogenetic inhibition of PV-INs also prevented the suppression of sucrose self-administration caused by TMT (**m**), yohimbine (**n**), and extinction learning (**o**) (TMT: interaction: $F_{1,14}=5.34$, $P=0.04$; yohimbine: group: $F_{1,14=}10.93$, $P=0.01$; extinction: interaction: $F_{1,12=}29.91$, $P=0.001$). CP-AMPAr, calcium-permeable AMPA receptor; oeEPSC, optically evoked excitatory postsynaptic current; SA, self-administration; WT, wild-type; Yoh, yohimbine; Group comparisons: *$P<0.05$, **$P<0.01$, ****$P<0.001$.

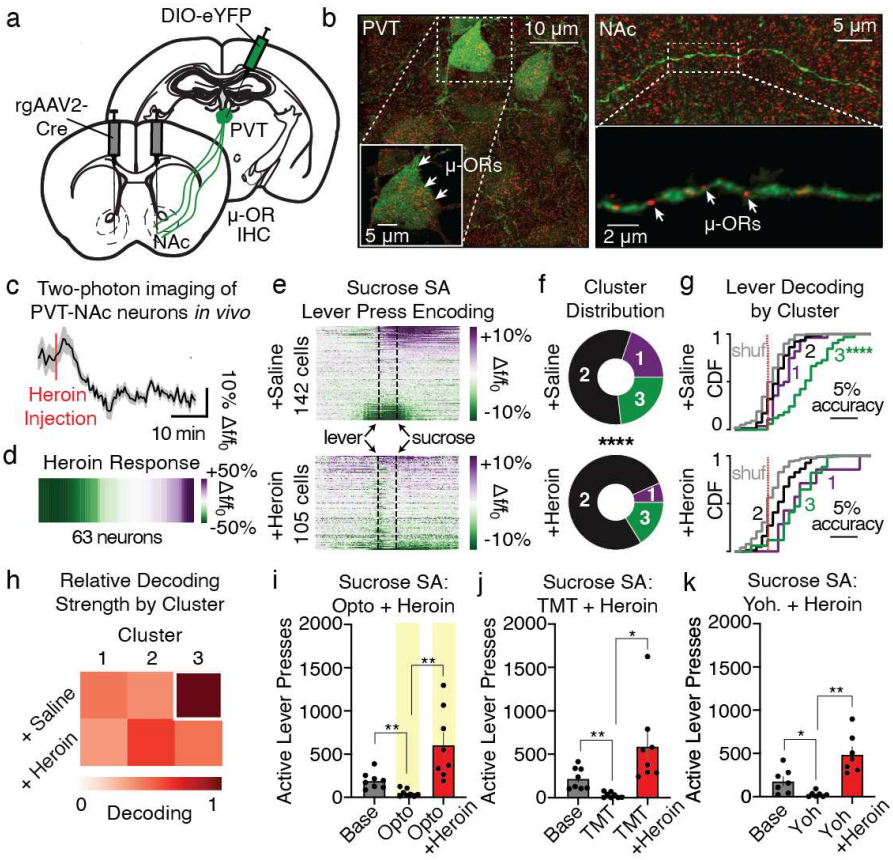

Figure 4. PVT→NAc dependent suppression of reward seeking is disrupted by an injection of heroin.

a-b, Surgical strategy (**a**) and IHC (**b**) revealed μ-opioid receptor expression on PVT→NAc somata and terminal axons. **c-d,** Averaged trace and heat map from two-photon calcium imaging *in vivo* reveal that heroin reduced the activity of PVT→NAc neurons (n=63 neurons/3 mice; t_{61} = 3.03, *P*=0.004). **e**, Heatmaps for all neurons during sucrose self-administration following injection of saline (top; n=142 cells/4 mice) or heroin (bottom; n=105 cells/4 mice). **f**, The proportion of cells in the excited ensemble (1) and inhibited ensemble (3) were significantly lower in heroin-injected mice versus saline-injected mice (χ^2=23.5, p<0.0001). **g**, Decoding shows that heroin reduced PVT→NAc neuronal decoding of active lever pressing. **h**, Heat maps depicting the active lever press decoding accuracy of each ensemble, which was superior for the inhibited ensemble (3) following an injection of saline, but not heroin. Decoding accuracy is normalized such that the best decoding equals a value of 1, whereas no decoding equals a value of 0. **i-k**, Heroin prevented the suppression of sucrose self-administration (n=7-8 mice/group) caused by PVT→NAc stimulation (**i**), TMT (**j**), and yohimbine (**k**) (Opto: $F_{2,21=}$11.56, *P*=0.004; TMT: $F_{2,21=}$8.77, *P*=0.002; yohimbine: $F_{2,18=}$16.36, *P*<0.001). μ-OR, μ-opioid receptor; IHC, immunohistochemistry; Base, Baseline; Opto, optogenetics; Yoh, Yohimbine. Group comparisons: **P*<0.05, ***P*< 0.01.

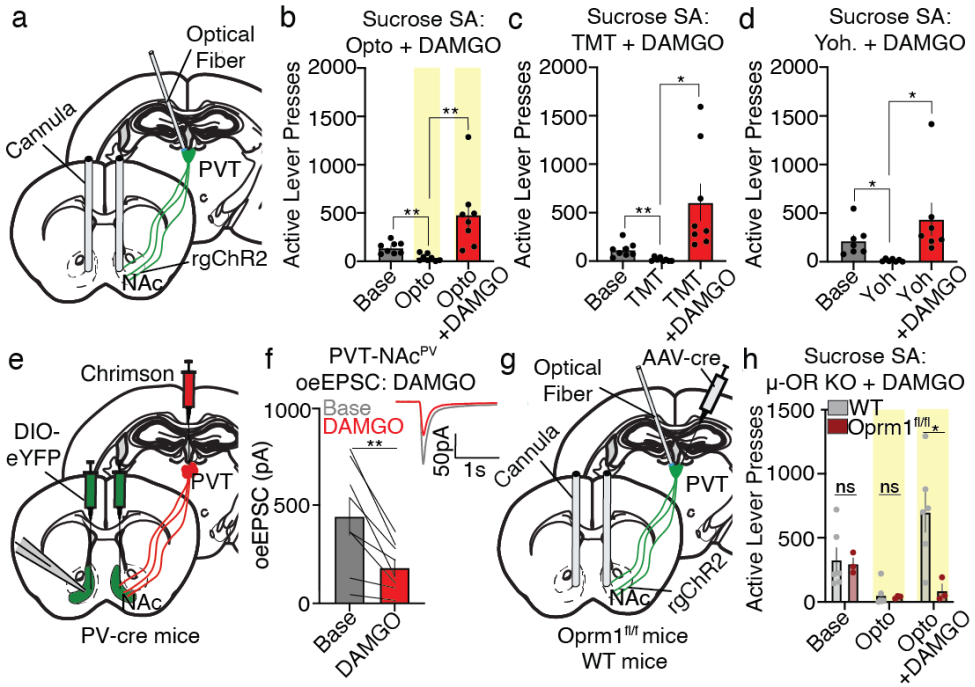

Figure 5. PVT→NAc dependent suppression of reward seeking is gated by presynaptic μ-opioid receptors.

a, Surgical strategy for simultaneous optogenetic manipulation of PVT→NAc neurons and intra-NAc DAMGO infusions. **b-d**, Intra-NAc infusion of DAMGO prevented the suppression of sucrose self-administration (n=7-8 mice/group) caused by PVT→NAc stimulation (**b**), TMT (**c**), and yohimbine (**d**) (Opto: $F_{2,21}$=9.33, *P*=0.001; TMT: $F_{2,21}$=8.02, *P*=0.003; yohimbine: $F_{2,18}$=4.26, *P*=0.03). **e**, Surgical strategy for patch-clamp electrophysiology. **f**, Example electrophysiological waveforms and grouped data reveal that μ-opioid receptor agonist DAMGO reduced PVT→$NAc^{PV\text{-}IN}$ oeEPSC amplitudes (n=8 cells/5 mice; t_7=4.12). **g**, Surgical strategy for PVT μ-opioid receptor knockout with simultaneous optogenetic manipulation of PVT→NAc neurons and intra-NAc microinfusions. **h**, Knockout of PVT μ-opioid receptors in $Oprm1^{fl/fl}$ mice rescued the suppression of sucrose self-administration caused by optogenetic stimulation of PVT→NAc neurons in the presence of intra-NAc DAMGO infusions (n=3-6 mice/group; interaction: $F_{2,14}$=4.46, *P*=0.03). μ-OR, μ-opioid receptor; Base, Baseline; Opto, optogenetics; Yoh, Yohimbine; KO, knockout; Group comparisons: **P*<0.05, ***P*< 0.01.

Methods

Animals

All experiments were approved by the Institutional Animal Care and Use Committee (IACUC) at the Medical University of South Carolina in accordance with the NIH-adopted Guide for the Care and Use of Laboratory Animals. Adult male and female C57BL6/J wild-type, PV-Cre (B6.Cg-*Pvalbtm1.1(cre)Aibs*/J, Strain #012358)[52], D2-Cre (*Drd2*, line ER44, RRID:MMRRC_017263-UCD)[53], and *Oprm1*$^{fl/fl}$ (B6.129-*Oprm1*$^{tm1.1Cgrf}$/KffJ, Strain #030074)[54] mice were group-housed pre-operatively and single-housed post-operatively, with access to standard chow and water *ad libitum* throughout all experiments (mice were at least 8 weeks of age and 20g prior to study onset). Mice were housed under a reverse 12:12-hour light cycle (lights off at 8:00am), with experiments performed during the dark phase.

Surgery

For cranial surgeries, all mice were anesthetized with isoflurane (0.8-1.5% in oxygen; 1L/minute) and placed within a stereotactic frame (Kopf Instruments). Ophthalmic ointment (Akorn), topical anesthetic (2% Lidocaine; Akorn), analgesic (Ketorolac, 2 mg/kg, ip), and subcutaneous sterile saline (0.9% NaCl in water) were given pre- and intra-operatively for health and pain management. An antibiotic (Cefazolin, 200 mg/kg, sc) was given post-operatively to reduce the possibility of infection, and mice were allowed to recover for at least 3 weeks after surgeries.

Two-photon calcium imaging: We targeted PVT→NAc projection neurons for two-photon calcium imaging through a single microinjection of a Cre-inducible virus encoding the calcium indicator GCaMP6m (AAVdj-ef1a-DIO-GCaMP6m; 300nl) into the posterior PVT (AP: -1.58mm; ML: -1.13mm; DV: -3.30mm; 20° angle), along with bilateral microinjections of a retrogradely-trafficked virus encoding Cre-recombinase (rgAAV2-hSyn-Cre; 500nl) aimed for the anterior/medial NAc shell (AP: +1.45mm; ML: ± 0.65mm; DV: -4.65mm) in wild-type mice. A microendoscopic gradient refractive index lens (GRIN lens; 8mm long, 0.5mm diameter, Inscopix) was also implanted dorsal to the PVT injection site (AP: -1.58mm; ML: -1.13mm; DV: -3.00mm; 20° angle), allowing chronic visual access to PVT→NAc projection neurons[6,55]. A stainless-steel head ring was cemented around the GRIN lens using dental cement and skull screws for subsequent head fixation[25]. Histology confirmed that GRIN lens placements and GCaMP6m fluorescence allowed localized visualization of posterior PVT neurons post-mortem.

Behavioral optogenetics, chemogenetics, and neuropharmacology: We targeted PVT→NAc projection neurons for optogenetic manipulations using injection coordinates and volumes that were identical to two-photon calcium imaging experiments described above. Our first strategy was to give a single microinjection of a Cre-inducible virus encoding one of the three opsins (AAV5-ef1a-DIO-ChR2-eYFP; AAV5-ef1a-DIO-eNpHR3.0-eYFP; AAV5-ef1a-DIO-eYFP) into the posterior PVT, along with bilateral microinjections of the retrogradely-trafficked virus encoding Cre-recombinase into the NAc shell (rgAAV2-hSyn-Cre) of wild-type mice. When combining these experiments with chemogenetics, we instead injected a retrogradely trafficked virus encoding channelrhodopsin (rgAAV2-hSyn-ChR2-eYFP) bilaterally into NAc shell, along with bilateral microinjections of a Cre-inducible virus encoding an inhibitory DREADD[56,57] into the NAc shell (AAV5-hSyn-DIO-hM4D(Gi)-mCherry) of PV-Cre or wild-type control mice. We also used this surgical strategy for μ-opioid receptor knockout experiments, wherein mice received a retrogradely trafficked virus encoding channelrhodopsin (rgAAV2-hSyn-ChR2-eYFP) bilaterally in NAc shell, and an injection of a virus encoding Cre-recombinase (AAV5-hSyn-Cre) into PVT. For all optogenetics experiments, a custom-made optical fiber[58] was implanted dorsal to the PVT injection site (AP: -1.58mm; ML: -1.13mm; DV: -3.00mm; 20° angle), allowing laser-evoked perturbation

of activity in PVT→NAc projection neurons. For optogenetics experiments involving simultaneous chemogenetics or neuropharmacology, a bilateral double-barrel guide cannula (Plastics One: 26-gauge, 5mm length, 1.2mm barrel separation) was implanted dorsal to the anterior/medial NAc shell (AP: +1.45mm; ML: ± 0.60mm; DV: -4.15mm). A stainless-steel head ring was cemented around the optical fiber and/or guide cannula using dental cement and skull screws. Histology confirmed optical fiber placements and structure-localized fluorescence post-mortem.

Immunohistochemistry and slice electrophysiology: We targeted PVT→NAc projection neurons for both immunohistochemical and slice electrophysiological studies using injection coordinates and volumes that were identical to two-photon calcium imaging experiments described above. For immunohistochemistry, we gave a single microinjection of a Cre-inducible virus encoding eYFP (AAV5-ef1a-DIO-eYFP) into the posterior PVT, along with bilateral microinjections of a retrogradely-trafficked virus encoding Cre-recombinase into the NAc shell (rgAAV2-hSyn-Cre) of wild-type mice. For slice electrophysiology, we gave a single microinjection of a virus encoding a red-shifted excitatory opsin (AAV5-hSyn-ChrimsonR-tdTomato)[30] into the PVT, along with bilateral microinjections of a Cre-inducible virus encoding an eYFP into the NAc shell (AAV5-ef1a-DIO-eYFP) of D2-Cre or PV-Cre mice.

Head-fixed behavior

Self-administration: Experiments involving sucrose self-administration were performed based on a previous study wherein we developed a model of natural- and drug-reward seeking in head-restrained mice, enabling simultaneous two-photon calcium imaging[59]. After recovery from surgery, mice were habituated to head fixation during 30-minute sessions wherein levers were not presented. Acquisition: Mice next acquired sucrose self-administration through 14 daily 1-hour sessions, during which two levers were placed within forelimb reach. A press on the active lever, but not inactive lever, resulted in the presentation of a tone cue (8 kHz, 2s), followed by a gap in time (trace interval; 1s), and finally the delivery of a liquid sucrose reward (12.5µl; 12.5% mixed in tap water). A timeout period (20s) was given after each cue- and sucrose-reinforced active lever press, wherein active lever pressing had no effect. Mice were capped at 10 sucrose droplets on days 1-2 of acquisition, 20 sucrose droplets on days 3-4 of acquisition, and 40 sucrose droplets on days 5-14 of acquisition to match previous drug self-administration experiments (capping prevents drug overdose in those studies). Suppression: Following acquisition of lever pressing for sucrose, we used several methods to suppress active lever pressing behavior. We first used a predator odor to suppress sucrose self-administration, wherein mice were exposed to the fox feces derivative TMT (30 µL; 1% v/v ddH_2O) or vehicle (order counterbalanced) within their home cage for 15 minutes[60]. Mice were removed from their home cage after TMT or vehicle exposure, and immediately underwent a normal, uncapped 45-minute sucrose self-administration session. We also used a pharmacological stressor to suppress sucrose self-administration, wherein mice were given a systemic injection of yohimbine (0.625mg/kg, i.p.; Sigma Chemical)[60] or vehicle (order counterbalanced) 15 minutes before a normal, uncapped 45-minute sucrose self-administration session. Finally, we used extinction learning to suppress active lever pressing. Following at least 2 normal acquisition sessions (no stressors), mice were given daily 1-hour sessions wherein active lever pressing no longer resulted in cue or sucrose delivery until extinction criteria were reached. Extinction criteria were determined a priori[59], as (1) at least 10 days of extinction training and (2) 2 of the last 3 days at a maximum of 20% active lever pressing rate as compared with the last 2 days of acquisition.

Reinstatement: Following extinction learning, mice were given a cue-induced reinstatement test wherein active lever pressing resulted in tone cue presentation (as in acquisition), but not sucrose delivery. A timeout period (20s) was given after the onset of each cue, wherein active lever pressing did not result in cue delivery.

Real-time place preference

Real-time place preference was conducted using a standard 2-chamber conditioning apparatus that was partially divided by a partition which created two visually (white versus black walls) and texturally (rod versus grate flooring) distinct environments. Optogenetic manipulation of PVT→NAc neurons was performed in mice expressing ChR2 or eYFP (as described above). Real-time place preference was assessed over two consecutive testing sessions (one 15 min. session per day), where optogenetic light was counterbalanced between environments for each mouse and session. On the first testing day, eYFP and ChR2 mice received an intraperitoneal injection of saline immediately before being placed in between the two chambers. On the second testing day, eYFP and ChR2 mice received an intraperitoneal injection of heroin (1mg/kg; i.p.) immediately before being placed in between the two chambers. Place preference data was analyzed using two-way ANOVAs, followed by Sidak's post-hoc analyses, and paired t-tests.

Two-photon calcium imaging

Data collection and processing: We visualized GCaMP6m-expressing PVT→NAc projection neurons using a two-photon microscope (Bruker Nano Inc) equipped with a tunable InSight DeepSee laser (Spectra Physics, laser set to 920nm, ~100fs pulse width), resonant scanning mirrors (~30Hz framerate), a 20X air objective (Olympus, LCPLN20XIR, 0.45NA, 8.3mm working distance), and GaAsP photodetectors. In some cases, two fields of view (FOVs) were visible through the GRIN lens (separated by >75μm in the Z-axis to avoid signal contamination from chromatic aberration), in which case we recorded from each FOV during separate imaging sessions. Data were acquired without averaging using PrarieView software, converted into hdf5 format, and motion corrected using SIMA[61]. Following motion correction, a motion-corrected video and averaged time-series frame were used to draw regions of interest (ROIs) around dynamic and visually distinct cells using the polygon selection tool in FIJI[62]. Fluorescent traces for each ROI were then extracted using SIMA, and all subsequent analyses were performed using custom Python codes in Jupyter Notebook[6,24]. Two-photon imaging was performed during select acquisition sessions (early: days 1-2; middle: days 7-8; late: days 13-14) and extinction sessions (early: days 1-2; late: last 2 days) to simplify data analysis.

Data analysis: We quantified the average or 'basal' fluorescence of each neuron across time, as basal fluorescence can serve as a proxy for firing rates in tonically active cell populations[24,25], including PVT→NAc neurons[6]. Fluorescent traces were averaged across 5-minute bins and normalized to the first 5-minutes of each session. In the case of sucrose self-administration sessions, which were of varying length depending on the day and speed of intake, we compared first and last 5-minutes of each session. Data for each neuron was normalized to the 5-minute baseline averaged across neurons, allowing assessment of within-session adaptations. These data were compared across time and sessions using a two-way ANOVA, followed by Sidak's post-hoc analyses for between-session comparisons.

In addition to fluorescence adaptations within sessions, we aligned fluorescent traces of each neuron to active lever presses, including the 10-seconds beforehand, 3-seconds between the lever press and sucrose delivery, and 10-seconds after sucrose delivery. The 23-second fluorescent trace was averaged across trials and plotted as a peri-stimulus time heatmap across neurons. Due to the robust active lever pressing rates both late in acquisition and during cue-induced reinstatement, the resulting 2-dimensional arrays from those sessions were used to inform separate principal components analyses. The number of principal components were determined using the inflection point of a scree plot, which graphs the peristimulus time histogram of variance explained versus an increasing number

of principal components. The remaining principal components were then plotted into a subspace and used to inform the Scikit-learn function *sklearn.cluster.SpectralClustering*, a spectral clustering algorithm that uses a k-nearest neighbor connectivity matrix to identify unique cell clusters. Spectral clustering was chosen due to its improved performance for separating dynamic neuronal datasets as compared with other clustering algorithms[23,24]. Finally, a decoding analysis was used to determine how activity of each neuron could predict future active lever pressing behavior. A binary decoder was used through the Scikit-learn functions *sklearn.discriminant_analysis, sklearn.smv,* and *sklearn.decomposition*, informed by the fluorescence of each neuron during 2 epochs: 1-second before each active lever press vs a random 1-second baseline. As a control, these 2 epochs were randomly shuffled, and the decoding analysis was repeated. The decoding scores for each neuron was subtracted from the average of shuffled data for the corresponding neuronal ensemble, and the data was plotted against the shuffled data for all neurons. These data were compared across ensembles and corresponding shuffled data using a two-way ANOVA, followed by Sidak's post-hoc comparisons.

Behavioral optogenetics, chemogenetics, and neuropharmacology

Optogenetics: We used optogenetics to stimulate or inhibit the activity of PVT→NAc neurons during the expression of sucrose taking (late acquisition) and seeking (cue-induced reinstatement), and during the suppression of sucrose taking (TMT or yohimbine tests) and seeking (late extinction) as described above. For photoactivation experiments in ChR2 or control eYFP mice, the laser (473nm; ~10mW) was pulsed (5ms; 20Hz) every for 30-second intervals once/minute throughout the session. For photoinhibition experiments in eNpHR3.0 or control eYFP mice, the laser (532nm; ~10mW) was displayed (pure light, not pulsed) for 30-second intervals once/minute throughout the session. Because each laser manipulation had no effect in control eYFP mice, these data were collapsed across groups for each experiment.

Chemogenetics and neuropharmacology: We used site-specific chemogenetics and neuropharmacology to determine the function of NAc cell types and signaling mechanisms for the suppression of sucrose taking and seeking. For chemogenetics experiments, microinfusions of saline vehicle (0.9% NaCl in water; 0.3μL) or CNO (0.1μg in 0.3μL) were administered into NAc 5-minutes before each behavioral session (session order counterbalanced). For neuropharmacology experiments, microinfusions of the vehicle saline (0.3 μL/side), D1-receptor antagonist SCH-23390 (0.6 μg in 0.3 μL/side)[63], D2-receptor antagonist raclopride (3 μg in 0.3 μL/side)[63], CP-AMPAr antagonist IEM-1640 (0.3 μg in 0.3 μL)[31], or the μ-opioid receptor agonist DAMGO (0.15 μg in 0.3 μL)[42] were administered 5-minutes before each behavioral session (saline and antagonist session order counterbalanced).

Heroin Experiments: We tested the influence of systemically administered heroin (1 mg/kg; i.p.) on PVT→NAc neuronal activity and on behavior. Heroin was administered 5-minutes after the onset of two-photon imaging experiments, such that within-session adaptations could be evaluated. For behavioral experiments, heroin was administered immediately before sucrose self-administration or real-time place preference testing (note that sucrose self-administration was also coupled with two-photon imaging). Behavioral data were analyzed across groups and behavioral sessions using a two-way ANOVA, followed by Sidak's post-hoc comparisons when applicable.

Patch-clamp electrophysiology

Five weeks after surgery, mice were deeply anesthetized with isoflurane (1.5% in oxygen; 1L/minute) before transcardial perfusion with oxygenated, ice-cold sucrose-based cutting solution containing the following (in mM): 225 sucrose, 119.0 NaCl, 1.0 NaH_2PO_4, 4.9 $MgCl_2$, 0.1 $CaCl_2$, 26.2 $NaHCO_3$, 1.25 glucose (305-310 mOsm). Brains were rapidly removed and bathed in cutting solution,

while coronal sections 300μm thick were taken using a vibratome (Leica VT1200S). Sections were incubated in warm aCSF (32° C) containing the following (in mM): 119 NaCl, 2.5 KCl, 1.0 NaH_2PO_4, 1.3 MgCl, 2.5 $CaCl_2$, 26.2 $NaHCO_3$, 15 glucose (305-310 mOsm). After at least 1-hour of recovery, slices were constantly perfused with aCSF and visualized using differential interference contrast through a 40X water-immersion objective mounted on an upright microscope (Olympus BX51). Whole-cell patch-clamp recordings were obtained using borosilicate pipettes (~3-5MΩ) backfilled with a potassium gluconate-based internal solution composed of the following (in mM): 130 K-gluconate, 10 KCl, 10 HEPES, 10 EGTA, 2 $MgCl_2$, 2 ATP, 0.2 GTP (pH 7.35, mOsm 280) to characterize action potential waveforms and to measure the amplitude of PVT→NAc synaptic currents (mediated by AMPA receptors). Alternatively, recordings were obtained using a cesium methylsulfonate-based internal solution composed of the following (in mM): 117 Cs methanesulfonic acid, 20 HEPES, 2.8 NaCl, 5 TEA, 2 ATP, 0.2 GTP (pH 7.35, mOsm 280) to measure the amplitude of synaptic currents (mediated by AMPA receptors) and AMPA rectification.

Patch-clamp recordings were obtained from $eYFP^+$ (PV-INs in PV-Cre mice, D2-MSNs in D2-Cre mice) and $eYFP^-$ (putative D1-MSNs in D2-Cre mice) neurons surrounding the virus injection site in anterior/medial NAc shell. eYFP was visualized using a blue LED (<1mW) and a GFP epifluorescence filter set. In a subset of neurons, depolarizing current pulses (800ms; 50pA steps) were applied in current-clamp mode to confirm that recordings were from fluorescence-identified cell types. Specifically, PV-INs were confirmed based on their fast-spiking properties, whereas D1- and D2-MSNs were confirmed by their relatively limited spike frequency, ramping depolarization, and/or late spiking features. We also evaluated functional synaptic innervation from PVT to each of the NAc cell types. Visually identified NAc neurons were held at -70mV in voltage-clamp mode, and presynaptic ChrimsonR-tdT^+ axons from PVT were activated using a green LED (10ms pulse, 1mW) pulsed every 10-15 seconds. The peak amplitude of reliably evoked excitatory postsynaptic currents was measured for each neuron and compared across cell types using a one-way ANOVA followed by Sidak's post-hoc tests for between group comparisons. In a subset of recordings, we confirmed that optically evoked excitatory postsynaptic currents (oeEPSCs) were blocked by 10-minute bath application of the glutamatergic AMPA receptor antagonist DNQX (10μM). Additionally, we examined the influence of the CP-AMPAr antagonist IEM-1640 (50μM)[31] and μ-opioid receptor antagonist DAMGO (3μM)[64] on oeEPSC amplitudes through bath application for 25-mintues. For these pharmacological experiments, the average amplitude of the AMPA receptor-mediated oeEPSCs was taken from the first 5 minutes of recordings (before drug application) and the last 5-minutes of recordings (after drug application). Responses were compared across time and cell types using a two-way ANOVA, followed by Sidak's post-hoc tests for between group comparisons. AMPA rectification was measured using the cesium-based internal solution in voltage-clamp mode, with a GABA receptor antagonist picrotoxin (100μM)[13] and the NMDA receptor antagonist APV included in the perfusion aCSF (50μM)[13]. oeEPSCs were taken as above, with 5 sweeps averaged at a range of voltages (-80, -70, -50, -30, -10, +10, +30, +50 mV). Data were normalized to the peak oeEPSC at -80mV, and an AMPA rectification index was calculated for each neuron as $I_{+50mV}/-I_{-70mV}$ where I is the peak oeEPSC amplitude at each voltage. AMPA rectification was then compared across neurons using a one-way ANOVA, followed by Sidak's post-hoc tests for between group comparisons.

Immunohistochemistry

Free-floating 80μm coronal sections containing the PVT or NAc were blocked in 0.1M PBS with 2% Triton X-100 (PBST) with 2% normal goat serum (NGS, Jackson Immuno Research, Westgrove, PA) for 2 hours at room temperature with agitation. Sections were then incubated overnight at 4ºC with

agitation in the appropriate primary antisera (see Supplementary Table 1) diluted in 2% PBST with 2% NGS, washed 3 times for 5 minutes in PBST, then incubated in the appropriate secondary antisera diluted in PBST with 2% NGS for 4 hours at room temperature with agitation. All secondary antisera were raised in goat, conjugated to Alexa fluorophores, were used at a concentration of 1:1000, and were purchased from Invitrogen (Carlsbad, CA). Sections were then washed 3 times for 5 minutes in PBST, mounted on SuperFrost+ slides, and cover slipped with ProLong™ Gold Antifade. Slides were stored in a dark area. Brain sections were imaged using a Leica SP8 laser-scanning confocal microscope. Care was taken to only acquire images within dense fields of virally transduced neurons ($eYFP^+$) in the NAc. Simultaneously, we also imaged immunohistochemically (IHC) labeled markers for NeuN, pre-pro Enkephalin (ppENK), nNOS, Parvalbumin (PV), Choline acetyltransferase (ChAT), or μ-opioid receptors (μ-ORs). Each non-eYFP signal was processed in separate IHC runs. For detection of $eYFP^+$ cells, an OPSL 488nm laser line was used. For all other cell type markers, a Diode 638nm laser line was used for detection. During all imaging experimentation, a frame size of 1024x1024 was used and pinhole size, laser power, gain, and Z-step thickness were held constant throughout. For cell type-specific staining IHC and $eYFP^+$ cell counting experimentation, a 20X air objective was used. In both imaging modalities Z-step thickness was derived using Nyquist parameters to obtain optimal sampling for our quantitative analyses.

All image analyses were performed on 3D reconstructed Z-series data sets. Once deconvolved (Hyugens deconvolution, SVI) data sets were imported to Imaris (v 9.0, Bitplane) for cell counting. The "spot" tool in Imaris was used in a semi-automated manner to detect and quantify virally labeled eYFP+ cells as well as immunohistochemically labeled $nNOS^+$, $ppENK^+$, PV^+, or $ChAT^+$ cells. Next, Imaris was used to quantify the number of cells with coincident eYFP and, nNOS, ppENK, PV, or ChAT labeling. For each cell type investigated, raw cell counts were expressed relative to data set volume (μm^3), to create a cell/μm^3 index and to account for potential variation in tissue thickness. To determine the cellular identity of NAc neurons that receive PVT input, the number of $eYFP^+$ cells that were coincidently $ppENK^+$, PV^+, $ChAT^+$ or $nNOS^+$ were calculated and expressed as a percentage of the total $eYFP^+$ population within each field imaged, again using 3-5 data sets per animal, sampling each hemisphere, across 4 animals. With these data, we generated percentages of D2 ($ppENK^+$), PV, ChAT, and nNOS neurons in each field that receive PVT input (identified via eYFP expression). Given the known population density of D1 and D2 MSNs at approximately 95% of total cells and the relatively small population density of interneurons within the NAc, we summed each cell type average percentage and inferred that the remaining fraction of $eYFP^+$ NAc cells that did not show reactivity for ppENK, PV, ChAT or nNOS were putative D1 MSNs. For statistical analysis, IBM SPSS (version 24) was used to conduct comparisons between cell type across region via one-way ANOVAs, followed by planned contrasts for each subregion of interest (NAc core vs NAc shell), with PVT→NAc PV^+ neuron counts being serially compared to each additional marker (nNOS, ppENK, ChAT). For all planned contrasts, equal variances were not assumed.

Data availability

All data reported in this paper will be shared by the lead contact upon request.

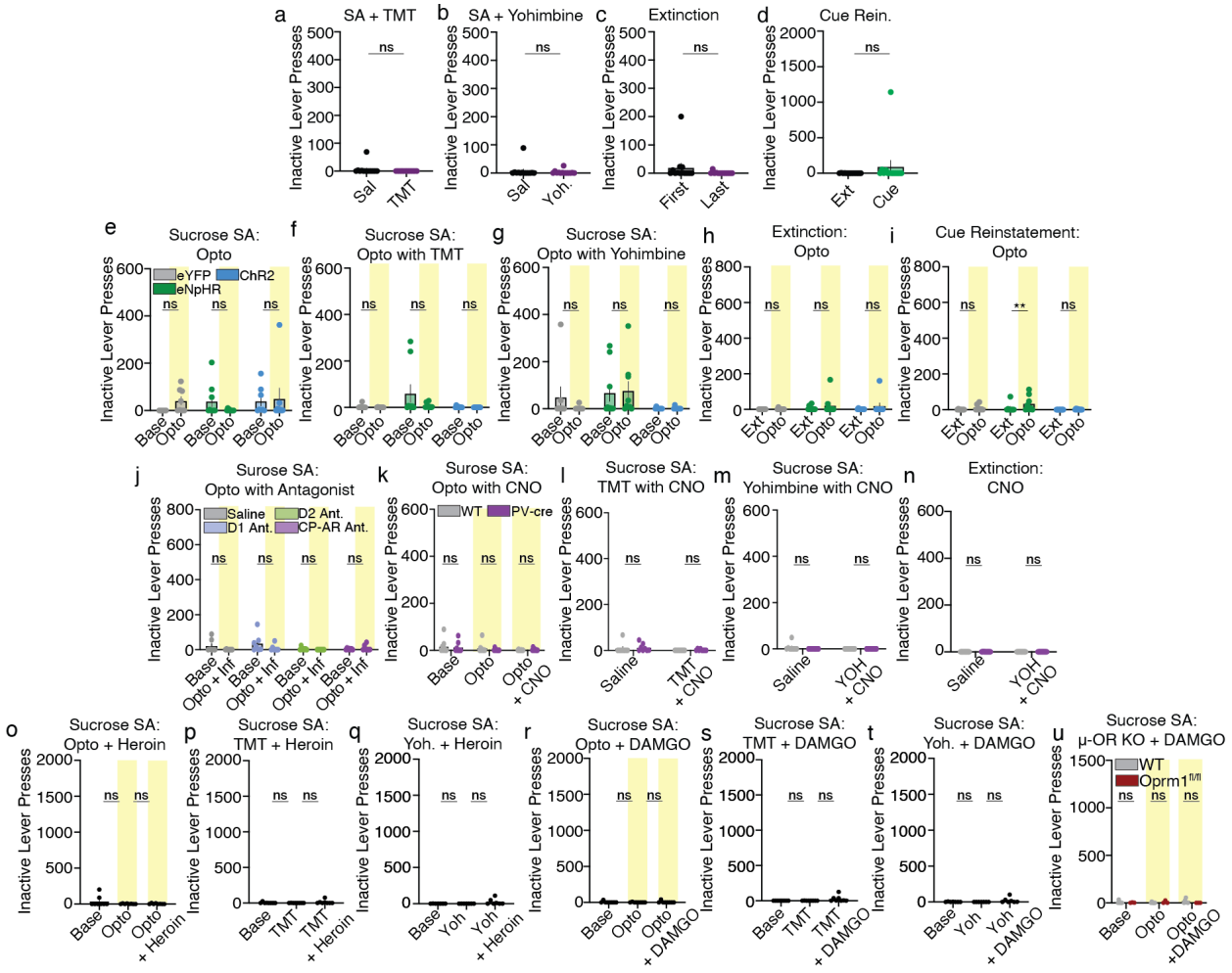

Supplementary Figure 1. Inactive lever pressing remained unchanged across conditions, suggesting goal-directed behavioral adaptations.

a-d, Inactive lever pressing remained unchanged after TMT exposure (**a**; TMT: t_{12}=1.08, *P*=0.30), yohimbine administration (**b**; t_{12}=0.63, *P*=0.54), extinction learning (**c**; t_{12}=1.32, *P*=0.21) and cue-induced reinstatement (**d**; t_{12}=1.09, *P*=0.29). **e-h**, Inactive lever pressing remained unchanged despite optogenetic manipulation of PVT→NAc neurons for opto (**e**; F-values<1.37, *P*-values>0.28), TMT (**f**; F-values<2.82, *P*-values>0.08), yohimbine (**g**; group: $F_{2,22}$=3.93, *P*=0.04; post-hoc: *P*-values>0.71), and extinction (**h**; F-values<1.68, *P*-values>0.21). **i**, Optogenetic inhibition of PVT→NAc neurons in eNpHR mice resulted in an increase of inactive lever pressing during cue-reinstatement, though other groups were unchanged (day: $F_{1,22}$=9.23, *P*=0.006; post-hoc: eNpHR ***P*=0.004). **j**, Inactive lever pressing remained unchanged despite optogenetic activation of PVT→NAc neurons with or without intra-NAc infusions of antagonists for D1 receptors, D2 receptors, and CP-AMPARs (F-values<3.61, *P*-values>0.07). **k-n**, Inactive lever pressing remained unchanged despite optogenetic manipulation of PVT→NAc neurons with or without chemogenetic inhibition of PV interneurons through intra-NAc infusions of CNO (**k**, opto: F-values<2.33, *P*-values>0.13; **l**, TMT: F-values<3.19, *P*-values>0.09; **m**, yohimbine: F-values<1.19, *P*-values>0.29; **n**, extinction: F-values<2.29, *P*-values>0.12). **o-t**, Inactive lever pressing remained unchanged across all conditions with or without a simultaneous systemic injection of heroin (**o**, opto: $F_{2,21}$=1.59, *P*=0.23; **p**, TMT: $F_{2,21}$=1.22, *P*= 0.32; **q**, yohimbine: $F_{2,18}$=2.25, *P*=0.13) or intra-NAc infusions of DAMGO (**r**, opto: $F_{2,21}$=0.32, *P*= 0.73; **s**, TMT: $F_{2,21}$=2.83, *P*=0.08; **t**, yohimbine: $F_{2,18}$=2.09, *P*=0.15). **u**, Inactive lever pressing remained unchanged for both WT and *Oprm1*$^{fl/fl}$ mice across all conditions ($F_{2,14}$=1.10, *P*=0.36).

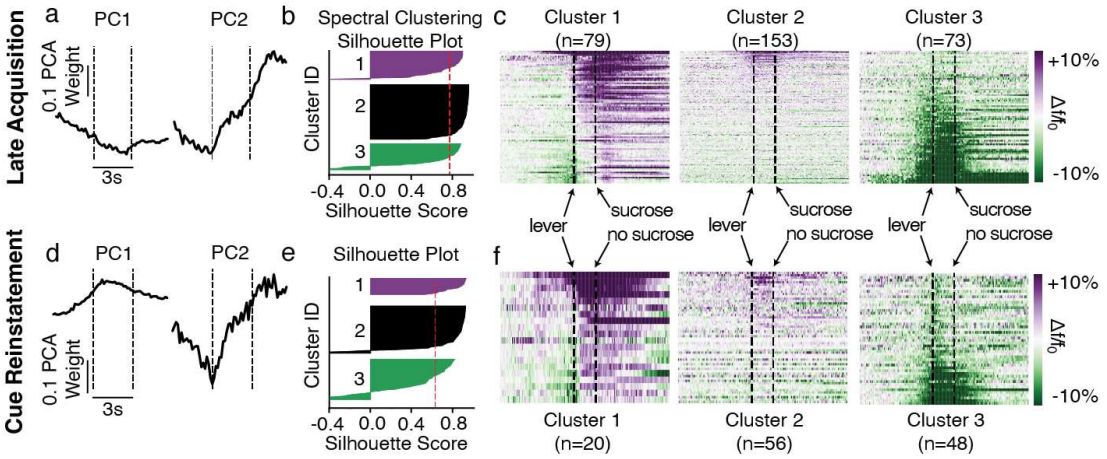

Supplementary Figure 2. PCA-based spectral clustering silhouette scores and within-cluster response dynamics.

a-b, Principal components analysis (**a**) and silhouette plot (**b**) show the relative fit for each neuron for each cluster formed by spectral clustering during late acquisition. **c**, Heatmaps for each neuronal ensemble reveals within-cluster neuronal responses during an active lever press for sucrose. **d-e**, Principal components analysis (**d**) and silhouette plot (**e**) show the relative fit for each neuron for each cluster during cue reinstatement. **f**, Heatmaps for each neuronal ensemble during an active lever press, with no sucrose reward.

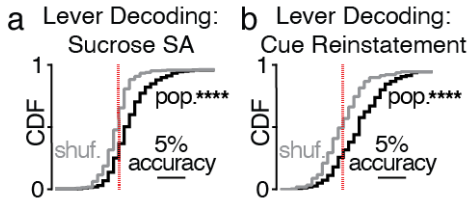

Supplementary Figure 3. Decoding reveals that PVT→NAc population dynamics can be used to predict active lever pressing.

a, CDF plot showing that the activity of all PVT→NAc neurons, not split by cluster, can predict active lever pressing during late acquisition (t_{304}=9.30, ****P<0.001). **b**, CDF plot showing all PVT→NAc neurons, not split by cluster, can predict active lever pressing during cue reinstatement (t_{123}=5.85, ****P<0.001).

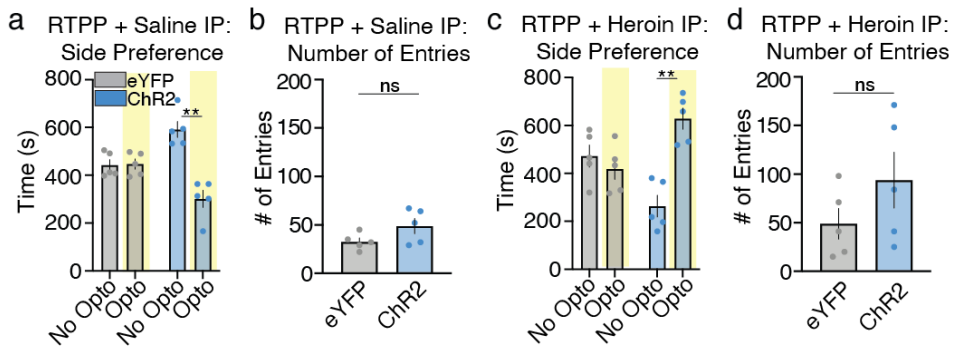

Supplementary Figure 4. Heroin administration causes stimulation of PVT→NAc neurons to be appetitive, rather than aversive.

a, Optogenetic stimulation of PVT→NAc neurons resulted in a real-time place aversion in ChR2 mice, but not eYFP mice (side x group: $F_{1,8}$=12.89, *P*=0.007; post-hoc: ChR2 ***P*=0.002, eYFP *P*=0.99). **b**, Optogenetic stimulation of PVT→NAc neurons did not affect locomotion, as there was not a significant difference in the number of chamber entries between eYFP and ChR2 mice (t_4=2.59; *P*=0.06). **c**, A single intraperitoneal injection of heroin resulted in stimulation-dependent real-time place preference in ChR2 mice, but not eYFP mice (side x group: $F_{1,8}$=10.85, P=0.01; post-hoc: ChR2 ***P*=0.007, eYFP *P*=0.82). **d**, Optogenetic stimulation of PVT→NAc neurons did not affect locomotion in heroin-treated mice, as there was not a significant difference in the number of chamber entries between eYFP and ChR2 mice (t_4=2.59; *P*=0.06).

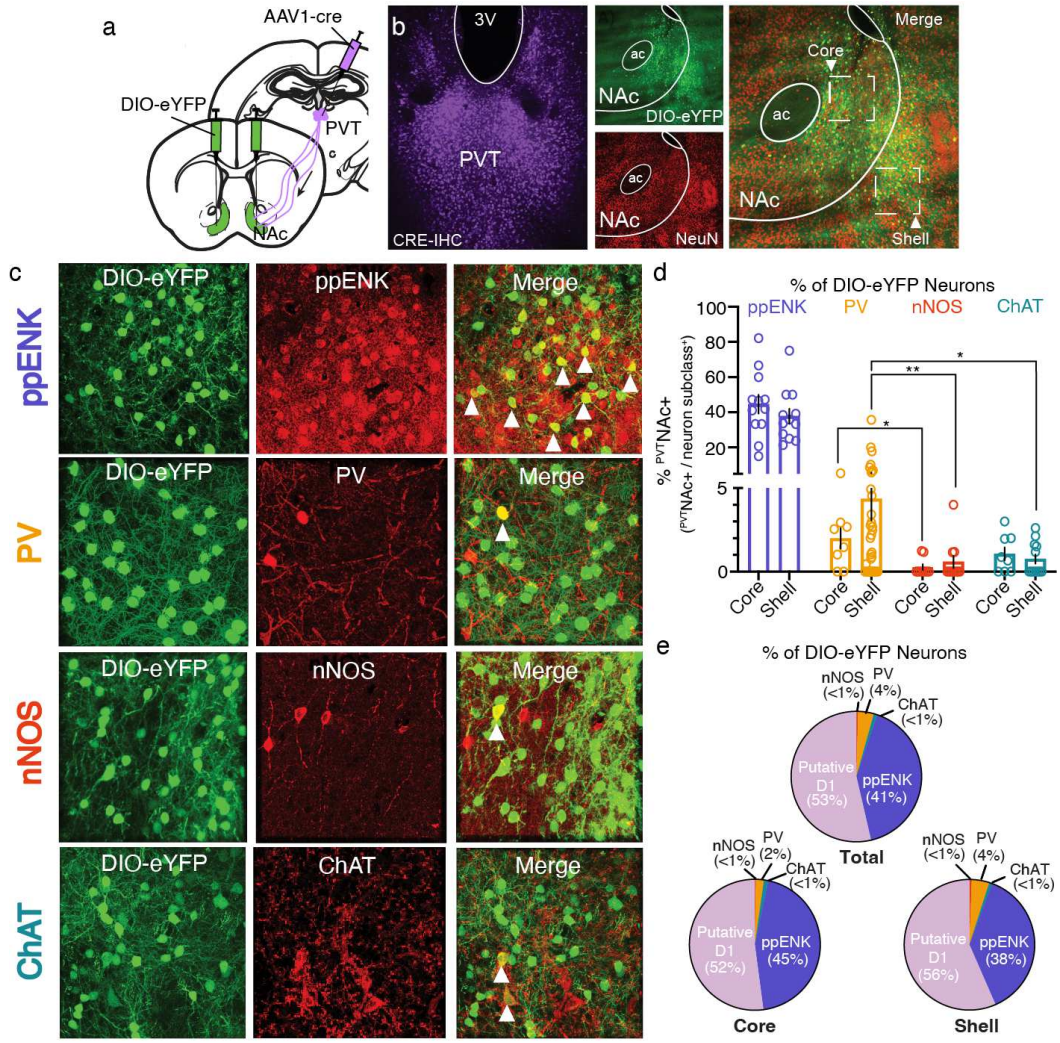

Supplementary Figure 5. Identification of downstream PVT projection targets reveals synaptic innervation of D1-MSNs, D2-MSNs, and PV interneurons.

a, Surgical strategy wherein the anterogradely trafficked virus AAV1-Cre[26] was used to label downstream cellular targets of PVT→NAc projection neurons. **b**, Example immunohistochemistry (IHC) for Cre, showing viral transduction of AAV1-Cre in posterior PVT (left); representative images of DIO-eYFP labeling and NeuN IHC in NAc core and shell (middle); merged image of Cre-inducible eYFP and NeuN in NAc (right). **c**, Representative images showing anterogradely labeled eYFP$^+$ neurons (left; neurons receiving strong PVT input), IHC for ppENK (putative D2 MSNs), PV, nNOS, and ChAT (middle), and overlayed images (right). **d**, Percentage of co-labeled eYFP$^+$ and neuron subclass markers in neurons of the NAc core versus shell. Anterograde PV interneuron labeling was elevated compared to other striatal interneurons in NAc shell (effect of cell type: $F_{3,64}$=61.39, P<0.001; PV vs nNOS, **P=0.008; PV vs ChAT, *P=0.01), but only greater than one striatal interneuron subtype in NAc core (effect of cell type: $F_{3,32}$=41.42, P<0.001; PV vs nNOS, *P=0.03; PV vs ChAT, P=0.28). **e**, Pie-charts displaying a comparison of eYFP$^+$/neuron subclass labeled markers in NAc core and shell; putative D1, D2-MSNs, and PV-interneurons had elevated anterograde labeling, suggesting strong synaptic connections with PVT.

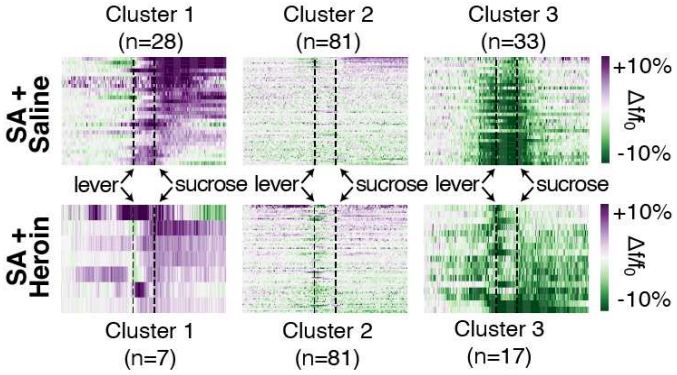

Supplementary Figure 6. Heroin administration limits PVT-NAc neuronal ensemble dynamics for reward-seeking behavior.

Heatmaps for each neuronal ensemble during sucrose self-administration following an intraperitoneal injection of saline (top; n=142 cells/4 mice) or heroin (bottom; n=105 cells/4 mice).

916 **Supplementary Table 1. Primary resources for immunohistochemistry.**

Primary antisera	Host species	Concentration	Source	RRID (AB_)	Immunogen	Secondary antisera
Choline acetyltransferase	Mouse	1:1000	Millipore, AMAB91130	2665812	Peptide sequence	Anti-mouse 647
Parvalbumin	Mouse	1:1000	Millipore, MAB1572	2174013	Parvalbumin purified from frog muscle	Anti-mouse 647
Pre-pro Enkephalin	Rabbit	1:200	Neuromics, RA14124	2532106	Peptide sequence	Anti-rabbit 647
nNOS	Rabbit	1:1000	Millipore, AB5380	91824	Recombinant human nNOS	Anti-rabbit 647
μ-Opioid Receptor	Rabbit	1:1000	Neuromics, RA10104	2156526	Peptide sequence	Anti-rabbit 647
NeuN	Mouse	1:1000	Millipore, MAB377	2298772	Purified cell nuclei	Anti-mouse 647
Cre	Mouse	1:1000	Millipore MAB3120	2085748	Cre-recombinase fusion protein	Anti-mouse 647